Optically induced transition between discrete and gap solitons in a nonconventionally biased photorefractive crystal

Peng Zhang,[1] Sheng Liu,[1] Jianlin Zhao,[1,*] Cibo Lou,[2] Jingjun Xu,[2] and Zhigang Chen[2,3]

[1]*Institute of Optical Information Science and Technology and Shaanxi Key Laboratory of Optical Information Technology, School of Science, Northwestern Polytechnical University, Xi'an 710072, China*

[2]*Key Laboratory of Weak-Light Nonlinear Photonics, Ministry of Education and TEDA Applied Physics School, Nankai University, Tianjin 300457, China*

[3]*Department of Physics and Astronomy, San Francisco State University, San Francisco, California 94132, USA*

[*]*Corresponding author: jlzhao@nwpu.edu.cn*

Received November 26, 2007; revised February 3, 2008; accepted February 21, 2008; posted March 4, 2008 (Doc. ID 90106); published April 14, 2008

We show that optically induced photonic lattices in a nonconventionally biased photorefractive crystal can support the formation of discrete and gap solitons owing to a mechanism that differs from the conventional screening effect. Both the bias direction and the lattice orientation can dramatically influence the nonlinear beam-propagation dynamics. We demonstrate a transition from self-focusing to -defocusing and from discrete to gap solitons solely by adjusting the optical-beam orientation. © 2008 Optical Society of America

OCIS codes: 190.6135, 190.4420.

Optical waves propagating in photonic lattices have attracted a great deal of research interest [1,2]. Photonic lattices created by optical induction method exhibit large reconfigurability for controllable linear and nonlinear propagations at moderate laser powers [3–9]. Such induced lattices provide ideal settings for studying the basic properties of wave propagation in periodic structures. By far, photorefractive (PR) crystals biased with an electric field have been one of the most popular materials for demonstrating a variety of discrete phenomena, including lattice solitons [3–7], bandgap guidance by defects [8], and Anderson localization in disordered lattices [9]. In all these studies, the experiments were performed in *conventionally* biased PR crystals, where self-focusing or self-defocusing nonlinearity was achieved by reversing the polarity of the external bias field.

Recently, we proposed to use a *nonconventionally biased* (NCB) PR crystal for the generation of elliptical bright solitons in homogenous media [10]. It was shown that, in the continuum case, spatial solitons can exist in a NCB crystal but with much richer dynamics, depending on the relative orientations of the crystalline c axis, the bias field, and the beam polarization. In this Letter, we report our theoretical and experimental results on the formation of one-dimensional (1D) lattice solitons under NCB conditions. We found that photonic lattices and lattice solitons can also be established under these conditions, but owing to a mechanism quite different from the conventional screening effect. Even surprisingly, switching between self-focusing and -defocusing nonlinearities can be achieved solely by changing the optical-beam orientation, thus facilitating the observation of transition between discrete and gap solitons without the need of reversing the polarity of the bias electric field.

We first formulate a dimensionless model to describe the nonlinear propagation of an optical (probe) beam in an optically induced 1D photonic lattice under NCB conditions. Figure 1(a) depicts our coordinate system, where the y axis is parallel to the direction of the intensity gradients ∇I of the stripe probe beam and the lattice beam and both beams propagate collinearly along the z axis. The angles of the bias field E_0 and ∇I with respect to the crystalline c axis are denoted by θ_e and θ_I, respectively. Then the steady-state propagation of the probe beam in the induced photonic lattice is governed by [3–5,10–12]

$$\left(\frac{\partial}{\partial z}-\frac{\mathrm{i}}{2}\frac{\partial^2}{\partial y^2}\right)B(y,z)=\mathrm{i}\left[|E_0|K(\theta)\frac{I_l+|B(y,z)|^2}{1+I_l+|B(y,z)|^2}-|E_0|\cos\theta_e\right]B(y,z), \quad (1)$$

where $K(\theta)=\cos(\theta_I-\theta_e)\cos\theta_I$, $B(y,z)$ is the amplitude of the extraordinarily polarized probe beam and $I_l=I_{l0}\cos^2(\pi y/d)$ is the intensity of the ordinarily polarized lattice beam.

According to the linear electro-optic effect, it can be easily obtained that only the c-axis component of an electric field can introduce perceptible index modulation in a PR crystal, and the induced rotation of the crystalline c axis due to other components can be neglected. To establish our theoretical model, we consider only the c-axis component of the electric field and take the crystal as a uniaxial crystal for NCB conditions. Under the above assumptions, the PR process in a NCB crystal can be described as follows. First, the c-axis component of the bias field E_{0c} introduces a uniform index change $\Delta n_0 \propto -|E_0|\cos\theta_e$ in the crystal. Second, the light-excited charge carriers separate under the effective bias field E_{eff} [11] to form a space-charge field E_s. Third, the c-axis component of E_s, i.e., E_{sc}, causes an index change $\delta n \propto |E_0|K(\theta)I/(1+I)$ in addition to Δn_0, where I is light intensity. Thus total index change Δn in the crystal is equal to $\Delta n_0+\delta n$. Since Δn_0 is uniform, the types of

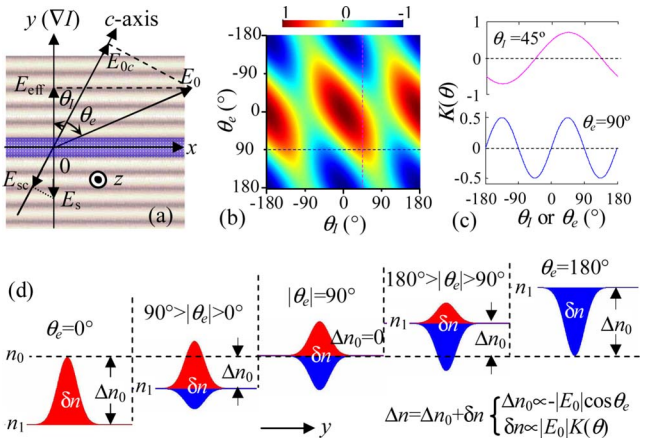

Fig. 1. (Color online) (a) Geometry of the coordinate system; (b) $K(\theta)$ versus θ_e and θ_I; (c) $K(\theta)$ versus θ_e at $\theta_I=45°$ (top) and $K(\theta)$ versus θ_I at $\theta_e=90°$ (bottom); (d) distributions of δn.

the nonlinearities of the crystal, no matter the sign and amplitude of Δn_0, depend solely on the sign of δn and thus on $K(\theta)$, i.e., $K(\theta)>0$ (<0) leads to self-focusing (-defocusing).

According to different geometric orientations, $K(\theta)$ has different values. Figures 1(b) and 1(c) depict $K(\theta)$ versus θ_e and θ_I. In Fig. 1(c), the regions under the dashed lines correspond to the self-defocusing cases. It can be seen from Figs. 1(b) and 1(c) that a switch between self-focusing and -defocusing can be achieved by altering either the bias direction or the beam orientation. To illustrate the essential differences between the conventional and nonconventional cases intuitively, we summarize the index changes induced by a Gaussian probe beam in the crystal under different bias conditions in Fig. 1(d), where for a fixed θ_e, the amplitude of δn varies with θ_I, and the shaded regions depict the variation ranges of δn. By setting $\theta_e=\theta_I=0°$ or 180°, the NCB case governed by Eq. (1) will be degenerated into the conventional one [see [5], Eq. (1)], and $\theta_e=0°$ (180°) corresponds to the self-focusing (-defocusing) nonlinearity [see Fig. 1(d)], in which the crystal index in the illuminated regions is less changed than that in the dark regions owing to the screening mechanism, and the variation ranges of the amplitude of δn coincide with the results presented in [11]. Under NCB conditions, the values of Δn_0 vary with θ_e [see the middle three columns in Fig. 1(d)]. In particular, at $|\theta_e|=90°$, $\Delta n_0=0$, reflecting a mechanism that is very different from the conventional screening effect. Furthermore, it is unexpected that, owing to the NCB fields, one can switch the type of the nonlinearities solely by changing θ_I, i.e., the optical-beam orientation. This will enable an optically induced transition between discrete and gap solitons without the need to reverse the bias field, as we shall demonstrate below.

Let us focus on a special case of NCB condition with $\theta_e=90°$, in which the bias field is perpendicular to the c axis. Under such a condition, $\theta_I=45°$ and $-45°$ correspond to the self-focusing and -defocusing cases, respectively [see Fig. 1(c)]. By solving Eq. (1), the numerical results for the evolutions of an input 1D Gaussian beam up to $z=2$ cm in induced photonic lattices are displayed in Fig. 2, where the top (bottom) row is for $\theta_I=45°$ ($-45°$). For these simulations, the parameters are chosen to match those from our experiments: The width of the probe beam is 10 μm (in FWHM), $d=20$ μm, and $E_0=400$ V/mm. The peak-intensity ratios of the probe and the lattice beam are 1:1.5 and 2:1 for the cases of $\theta_I=45°$ and $-45°$, respectively. Without nonlinearity, the probe beam undergoes discrete diffraction [Figs. 2(a1) and 2(b1)]. With nonlinearity, the balance between self-focusing or -defocusing and discrete diffraction leads to stable self-trapped states [Figs. 2(a2) and 2(b2)]. By comparing the interferograms shown in Figs. 2(a3) and 2(b3), it is obvious that $\theta_I=45°$ corresponds to a (semi-infinite gap) discrete soliton with a uniform phase structure and $-45°$ corresponds to a (Bragg reflection) gap soliton with a staggered phase structure.

To seek soliton solutions corresponding to the results shown in Fig. 2, we solve Eq. (1) in the form $B(y,z)=b(y)\exp(i\beta z)$, where β is a propagation constant, and the real envelope $b(y)$ satisfies the following equation:

$$\beta b(y)-\frac{1}{2}\frac{\mathrm{d}^2 b(y)}{\mathrm{d}y^2}=\left[|E_0|K(\theta)\frac{I_l+|b(y)|^2}{1+I_l+|b(y)|^2}-|E_0|\cos\theta_e\right]b(y). \quad (2)$$

Under linear conditions, the diffraction relation can be obtained by the Bloch–Floquet theory. With nonlinearity, the soliton solutions can be found by using numerical iteration procedures. The bandgap structures and typical soliton solutions are shown in Fig. 3. As expected, the propagation constants β for the discrete solitons lie in the semi-infinite gap, whereas those for the gap solitons reside in the first Bragg-reflection gap. The soliton peak intensity increases or decreases monotonously with β, while higher peak intensities correspond to stronger localizations.

The experimental setup for our demonstration is similar to that used in [6]. The photonic lattices are created in a SBN:60 crystal with dimensions of $5\times10\times5(c)$ mm^3 by sending a partially coherent beam ($\lambda=488$ nm) through an amplitude mask. An additional probe laser beam (taken from the same laser)

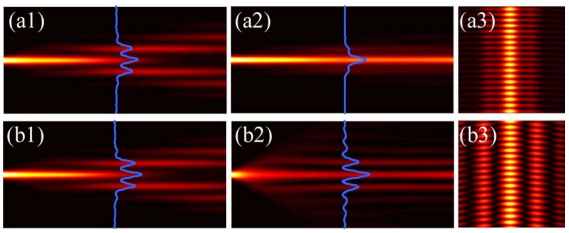

Fig. 2. (Color online) Linear (left) and nonlinear (middle) beam evolutions with $\theta_I=45°$ (top) and $-45°$ (bottom) at $E_0\perp c$. The curves in (a) and (b) depict beam profiles at $z=1$ cm. The right column corresponds to the interferogram of the nonlinear output beam at $z=1$ cm.

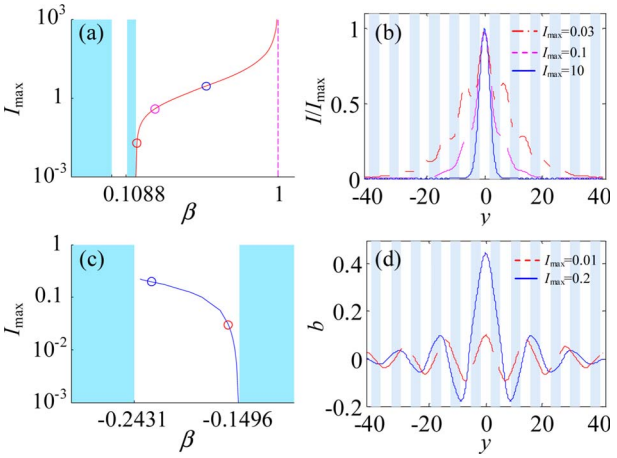

Fig. 3. (Color online) (a) and (c) bandgap structures (bands are shaded) and soliton peak intensity curves; (b) and (d) soliton profiles found at the circles marked in (a) and (c). The top and the bottom rows are for the cases with θ_I=45° and −45° at $E_0 \perp c$, respectively.

focused by a cylindrical lens propagates collinearly with the lattice beam. The amplitude mask and the cylindrical lens can each be rotated freely in the transverse plane. For observation of discrete and gap solitons, the intensity ratios between the probe beam (about 10 μm FWHM) and the lattice beam (about 20 μm spacing) are adjusted to be about 1:1.5 and 2:1, respectively. The polarization direction of the input probe (lattice) beam is adjusted to be parallel (perpendicular) to the c axis, and the bias direction is perpendicular to the c axis. To observe discrete diffractions and self-localized states of the probe beam, we first block off the probe beam until the lattice structures arrive in steady state. We then open the probe beam and monitor its linear-to-nonlinear evolution, taking advantage of the noninstantaneous response of the PR crystal [3–6].

Typical experimental results corresponding to Fig. 2 are shown in Fig. 4, where 4(a)–4(c) are the intensity patterns of the probe beam at input, linear output without lattice, and the lattice beam. Figure 4(d) illustrates the beam orientations for observing transition between discrete and gap solitons at $E_0 \perp c$, which are displayed in Figs. 4(e) and 4(f). For convenience of comparison, the beam patterns corresponding to Figs. 4(e) and 4(f) are all rotated in transverse plane by 45°. The bias voltages for observations of Figs. 4(e) and 4(f) are kept at the same 2.0 kV. It can be seen from Fig. 4 that, in the absence of nonlinearity, the probe beam undergoes discrete diffractions. While in the presence of nonlinearity, the probe beam evolves into self-localized states. The interferograms shown in Figs. 4(e3) and 4(f3) illustrate clearly that the discrete and gap solitons possess uniform and staggered phase structures, respectively. Remarkably, a perfect transition from self-focusing to self-defocusing [Figs. 4(e4) and 4(f4)] and from a discrete soliton to a gap soliton [Figs. 4(e3) and 4(f3)] is realized solely by adjusting the beam orientation. These observations are in good agreement with the numerical results.

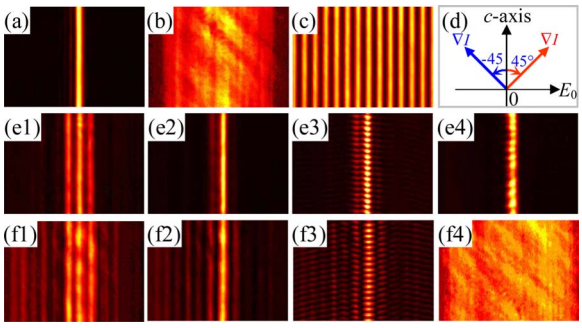

Fig. 4. (Color online) Experimental results. (a) and (b) Input and linear output probe beam pattern without lattice; (c) lattice beam pattern; (d) geometry of beam orientation; (e)–(f) probe-beam output pattern for (1) discrete diffraction, (2) self-trapping, (3) interference of soliton output, and (4) nonlinear output without lattice for (e) θ_I=45° and (f) −45° at $E_0 \perp c$, respectively.

In summary, we have demonstrated an optically induced transition from self-focusing and discrete solitons to self-defocusing and gap solitons without the need of electric bias reversal. Our results bring about a novel approach for bandgap engineering and diffraction management of light-induced photonic lattices. We expect that a similar approach could be applied to the 2D configuration, in which more-complicated wave phenomena are expected.

This work was supported by the NPU Foundation for Fundamental Research, the Doctorate Foundation of NPU, the 973 program, 111 project, NSFC, PCSIRT, NSF, and AFOSR. We thank L. Tang and C. Denz for discussions.

References

1. D. N. Christodoulides and R. I. Joseph, Opt. Lett. **13**, 794 (1988).
2. H. S. Eisenberg, Y. Silberberg, R. Morandotti, A. R. Boyd, and J. S. Aitchison, Phys. Rev. Lett. **81**, 3383 (1998).
3. J. W. Fleischer, T. Carmon, M. Segev, N. K. Efremidis, and D. N. Christodoulides, Phys. Rev. Lett. **90**, 023902 (2003).
4. J. W. Fleischer, M. Segev, N. K. Efremidis, and D. N. Christodoulides, Nature **422**, 147 (2003).
5. D. Neshev, E. Ostrovskaya, Y. Kivshar, and W. Królikowski, Opt. Lett. **28**, 710 (2003).
6. H. Martin, E. D. Eugenieva, Z. Chen, and D. N. Christodoulides, Phys. Rev. Lett. **92**, 123902 (2004).
7. D. Neshev, A. A. Sukhorukov, B. Hanna, W. Królikowski, and Y. Kivshar, Phys. Rev. Lett. **93**, 083905 (2004).
8. I. Makasyuk, Z. Chen, and J. Yang, Phys. Rev. Lett. **96**, 223903 (2006).
9. T. Schwartz, G. Bartal, S. Fishman, and M. Segev, Nature **446**, 52 (2007).
10. P. Zhang, J. Zhao, C. Lou, X. Tan, Y. Gao, Q. Liu, D. Yang, J. Xu, and Z. Chen, Opt. Express **15**, 536 (2007).
11. P. Zhang, Y. Ma, J. Zhao, D. Yang, and H. Xu, Appl. Opt. **45**, 2273 (2006).
12. A. A. Zozulya and D. Z. Anderson, Phys. Rev. A **51**, 1520 (1995).